Mafb lineage tracing to distinguish macrophages from other immune lineages reveals dual identity of Langerhans cells

Xiaodi Wu,[1] Carlos G. Briseño,[1] Vivek Durai,[1] Jörn C. Albring,[3] Malay Haldar,[4] Prachi Bagadia,[1] Ki-Wook Kim,[1] Gwendalyn J. Randolph,[1] Theresa L. Murphy,[1] and Kenneth M. Murphy[1,2]

[1]Department of Pathology and Immunology and [2]Howard Hughes Medical Institute, Washington University School of Medicine, St. Louis, MO 63110
[3]Department of Medicine A, Hematology and Oncology, University of Münster, 48149 Münster, Germany
[4]Department of Pathology and Laboratory Medicine, Abramson Family Cancer Research Institute, Perelman School of Medicine, University of Pennsylvania, Philadelphia, PA 19104

Current systems for conditional gene deletion within mouse macrophage lineages are limited by ectopic activity or low efficiency. In this study, we generated a *Mafb*-driven Cre strain to determine whether any dendritic cells (DCs) identified by *Zbtb46*-GFP expression originate from a *Mafb*-expressing population. Lineage tracing distinguished macrophages from classical DCs, neutrophils, and B cells in all organs examined. At steady state, Langerhans cells (LCs) were lineage traced but also expressed *Zbtb46*-GFP, a phenotype not observed in any other population. After exposure to house dust mite antigen, *Zbtb46*-negative CD64$^+$ inflammatory cells infiltrating the lung were substantially lineage traced, but *Zbtb46*-positive CD64$^-$ cells were not. These results provide new evidence for the unique identity of LCs and challenge the notion that some inflammatory cells are a population of monocyte-derived DCs.

The Journal of Experimental Medicine

INTRODUCTION

Classical DCs represent a discrete lineage distinguishable in ontogeny and function from macrophages (Merad et al., 2013). Previously, we and others observed that *Zbtb46* expression is a trait shared by all classical DCs and not shared by macrophages (Meredith et al., 2012; Satpathy et al., 2012a). However, no single transcriptomic or functional characteristic is sufficient to distinguish the classical, plasmacytoid, and monocyte-derived subsets of DCs taken as a whole from macrophage subsets (Hume et al., 2013).

The biology of monocyte-derived DCs (moDCs) is of considerable interest because of their use in many human DC-based cancer immunotherapies (Anguille et al., 2014). It is clear that monocytes isolated from the mouse can differentiate into moDCs upon treatment with GM-CSF and IL-4 (Inaba et al., 1992; Sallusto and Lanzavecchia, 1994) and acquire *Zbtb46* expression under such conditions (Satpathy et al., 2012a). Those mouse cells are a heterogeneous population comprising both macrophage-like and DC-like fractions (Helft et al., 2015), although it is unclear whether human moDCs in vitro are similarly heterogeneous. In the context of inflammation, cells that express the surface markers MHC class II (MHC-II), CD11c, and Ly-6C have been identified as in vivo moDCs (Langlet et al., 2012; Merad et al., 2013; Plantinga et al., 2013). Further, depletion of Ly-6C^{hi} monocytes using an anti-CCR2 antibody decreases the frequency of Ly-6C^{lo} *Zbtb46*-GFP$^+$ cells in the inflamed gut (Zigmond et al., 2012). Thus, moDCs may lose expression of Ly-6C and acquire expression of *Zbtb46* upon differentiation from monocytes (Zigmond et al., 2012); alternatively, Ly-6C^{hi} monocytes may help to recruit *Zbtb46*-expressing DCs. Some have suggested that Ly-6C$^+$ moDCs might be indistinguishable from monocyte-derived macrophages and myeloid-derived suppressor cells (Guilliams et al., 2014; Chow et al., 2016) or even from relatively undifferentiated monocytes (Jakubzick et al., 2013).

Langerhans cells (LCs) are branched, unpigmented, and slowly dividing cells resident in the epidermis with an unresolved relationship to other myeloid subsets (Satpathy et al., 2012b; Guilliams et al., 2014). They develop from embryonic monocytes and are replenished under inflammatory conditions by progenitors in the blood or BM (Merad et al., 2002; Ginhoux et al., 2006; Hoeffel et al., 2012; Seré et al., 2012). Like microglia, LCs are unaffected by loss of either the cytokine Flt3L or its receptor Flt3 and instead require IL-34 signaling through M-CSFR (Ginhoux et al., 2006, 2009; Kingston et al., 2009; Greter et al., 2012; Wang et al., 2012). However, like classical DCs and unlike macrophages, activated LCs increase migration to draining LNs (Silberberg-Sinakin et al., 1976), where they up-regulate expression of genes such as *Flt3* and *Zbtb46* (Miller et al., 2012;

Correspondence to Kenneth M. Murphy: kmurphy@wustl.edu

Abbreviations used: AF, Alexa Fluor; BV, Brilliant violet; EpCAM, epithelial cell adhesion molecule; FLP, flippase; FRT, FLP recognition target; HDM, house dust mite; *kr*, *kreisler*; LC, Langerhans cell; LPM, large peritoneal macrophage; MACS, magnetic-activated cell sorting; moDC, monocyte-derived DC; SPM, small peritoneal macrophage; UTR, untranslated region.

The Rockefeller University Press $30.00
J. Exp. Med. 2016 Vol. 213 No. 12 2553–2565
https://doi.org/10.1084/jem.20160600

Satpathy et al., 2012b). LCs that migrate out of human skin explants also express abundant *ZBTB46* mRNA (Artyomov et al., 2015), and depletion of *Zbtb46*-expressing cells decreases the frequency of LCs among cells that migrate out of mouse skin explants and among cells within mouse draining LNs (Mollah et al., 2014). In other respects, LC migration at steady state is poorly understood (Kaplan, 2010), in part because the genetic models used in some studies cannot distinguish LCs from other lineages. For example, a langerin-driven fluorescent reporter developed to track LCs also labels classical DCs in the dermis (Kissenpfennig et al., 2005; Bursch et al., 2007; Ginhoux et al., 2007; Poulin et al., 2007). Similarly, lineage tracing using LysM-Cre labels DCs in the dermis along with langerin-expressing cells in the draining LN (Jakubzick et al., 2008).

For those reasons, we sought to examine whether a macrophage reporter model could clarify the various origins of *Zbtb46*-expressing DCs observed in vivo. Currently available systems do not permit conditional gene deletion strictly within macrophage lineages (Abram et al., 2014). For example, LysM-Cre (Clausen et al., 1999) promotes significant deletion in macrophages and neutrophils, and F4/80-Cre (Schaller et al., 2002) deletes incompletely among macrophage populations (Abram et al., 2014). CD11c-Cre (Caton et al., 2007) deletes robustly in alveolar macrophages and in classical and plasmacytoid DCs, whereas *Cx3cr1*-Cre deletes in many subsets of macrophages and classical DCs (Abram et al., 2014). Thus, we set out to design a new lineage-tracing model that would be more faithfully restricted to macrophages to study the overlap between macrophage populations and *Zbtb46*-expressing DCs.

RESULTS AND DISCUSSION

Generation of a *Mafb*-driven lineage-tracing model

Using principal component analysis to compare gene expression in macrophages and DCs, we proposed that a reporter based on expression of the gene that encodes transcription factor MafB could distinguish macrophages from DCs (Satpathy et al., 2012b). In myeloid progenitors, MafB represses erythroid and DC fate (Kelly et al., 2000; Bakri et al., 2005). In resident macrophages, MafB and its paralog c-Maf repress a network of self-renewal genes and are transiently downregulated during cell proliferation (Soucie et al., 2016). Tumor-associated myeloid cells have been identified as macrophages rather than DCs partly on the basis of *Mafb* mRNA expression (Franklin et al., 2014).

We targeted C57BL6/N mouse embryonic stem cells to insert sequences encoding FLAG-tagged mCherry fluorescent protein and Cre recombinase into the endogenous *Mafb* locus. We used sequences encoding self-cleaving 2A peptides (Ryan et al., 1991; Szymczak-Workman et al., 2012) to separate those exogenous protein-coding sequences from each other and from the endogenous single-exon *Mafb* coding sequence preserved upstream (Fig. 1). Our in-frame knock-in targeting strategy was

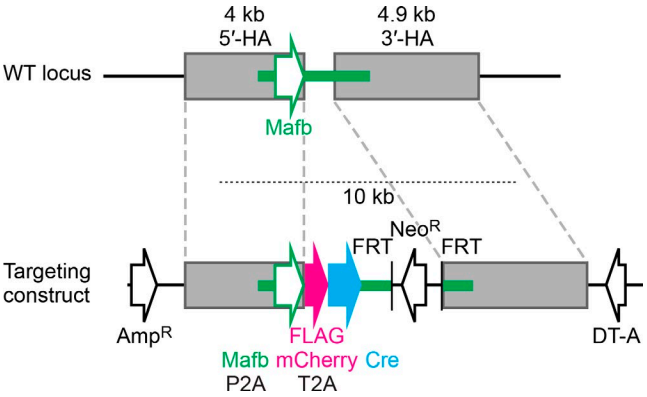

Figure 1. **Targeting strategy to generate MafB-mCherry-Cre knock-in mice.** Arrows indicate orientation of coding sequences, and green bars indicate UTRs. Amp^R, ampicillin resistance; DT-A, diphtheria toxin fragment A; HA, homology arm; Neo^R, neomycin resistance.

informed by observations that protein synthesis rate and mRNA abundance together explain the vast majority of variation in protein abundance (Schwanhäusser et al., 2011; Li et al., 2014; Jovanovic et al., 2015). In using 2A peptides that yield almost stoichiometric protein coexpression (Szymczak-Workman et al., 2012), our aim was to generate an allele that recapitulates the characteristics of wild-type *Mafb* in transcription and translation.

Our attention to faithful expression of MafB from the mutated allele was prompted by evidence that *Mafb*-haploinsufficient mice exhibit subtle defects in hematopoiesis (Sultana et al., 2009) and by reports that aberrant expression of that protein can severely decrease viability of the organism. The *kreisler* (*kr*) mutation is a radiation-induced chromosomal inversion that separates an intact *Mafb* transcriptional unit from putative distal enhancer elements (Cordes and Barsh, 1994). Mice homozygous for the *kr* mutation rarely survive to sexual maturity and show gross behavioral deficits caused by abnormalities in hindbrain and inner ear development (Hertwig, 1942; Cordes and Barsh, 1994). In contrast, mice homozygous for our targeted allele (which we call MafB-mCherry-Cre) survived into adulthood and were reproductively competent. They showed behavior indistinguishable from wild-type littermates, never manifesting the circling or dancing movement disorder observed in *kr/kr* mice (Hertwig, 1942). These observations suggest that regulation of the *Mafb* locus was minimally altered by the in-frame insertion of sequences encoding mCherry and Cre.

To generate lineage-tracing mice, we first crossed *Zbtb46*-GFP mice (Satpathy et al., 2012a) to R26-stop-YFP mice, which have a loxP-flanked stop sequence upstream of an enhanced YFP gene inserted into the constitutive and ubiquitous *Gt(ROSA)26Sor* locus (Srinivas et al., 2001); we then crossed either those progeny or R26-stop-YFP mice to MafB-mCherry-Cre mice.

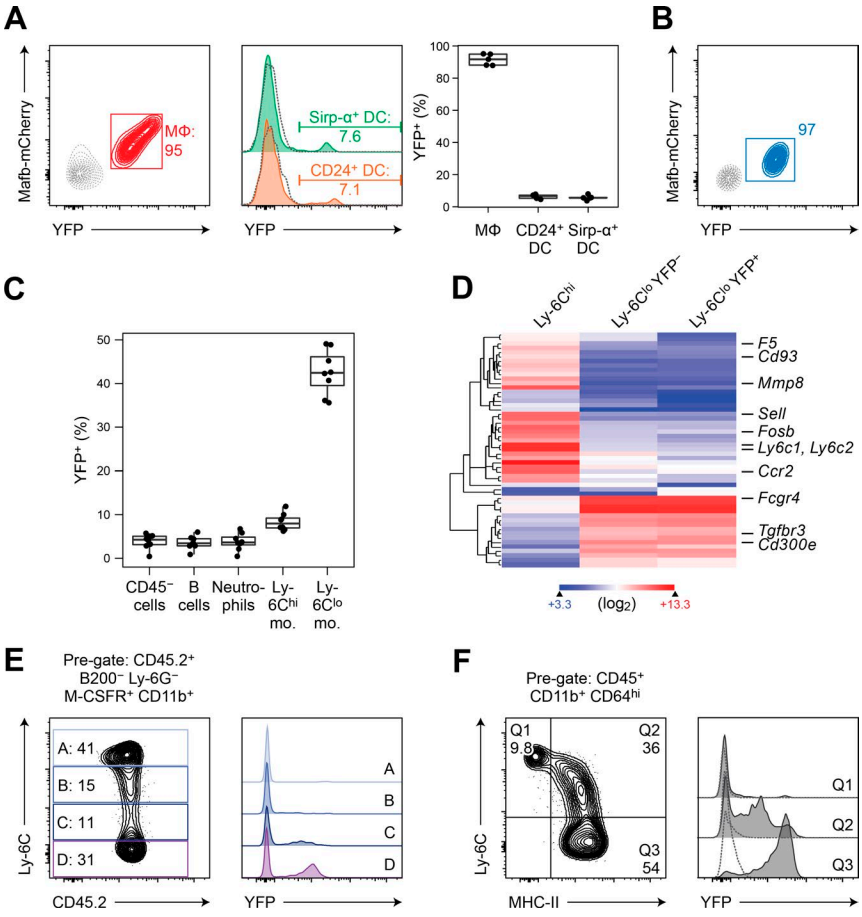

Figure 2. **Monocyte progeny are marked by *Mafb*-driven lineage tracing.** (A) Macrophages (MΦ) in MafB-mCherry-Cre × R26-stop-YFP × *Zbtb46*-GFP mouse spleen, gated as in Fig. S1 A, are displayed for expression of *Mafb*-mCherry and lineage-tracing marker YFP in a two-color histogram, and classical DC subsets are compared for expression of YFP. Shown is one sample and a box plot representing first quartile, median, and third quartile frequencies ($n \geq 5$ animals over at least three independent experiments). (B) Microglia in MafB-mCherry-Cre × R26-stop-YFP mouse brain, gated as in Fig. S1 B, are displayed for expression of Mafb-mCherry and YFP in a two-color histogram. Shown is one representative sample ($n \geq 3$ animals over at least two independent experiments). (A and B) Numbers indicate percentage of cells within the indicated gate, and dotted gray lines show fluorescent signal measured in non-mCherry and non-YFP control samples. (C) Lineages in MafB-mCherry-Cre × R26-stop-YFP × *Zbtb46*-GFP mouse blood, gated as in Fig. S1 C, are compared for expression of YFP. Shown is a box plot representing first quartile, median, and third quartile frequencies ($n \geq 8$ animals over at least four independent experiments). mo., monocytes. (D) Heat map showing relative gene expression in the indicated monocyte subsets for gene expression microarray probe sets differentially expressed in Ly-6C^{hi} and Ly-6C^{lo} monocytes. Shown are averages of two biological replicates, excluding one YFP$^-$ Ly-6C^{lo} monocyte sample below quality control thresholds. (E) Monocytes identified in C, distinguished on the basis of Ly-6C expression (left), are compared for expression of YFP (right). Shown is one representative sample. (F) Maturing macrophages in MafB-mCherry-Cre × R26-stop-YFP × *Zbtb46*-GFP mouse small intestinal lamina propria, identified by surface markers as indicated (left) after pregating as in Fig. S1 D, are compared for expression of YFP (right). Shown is one representative sample ($n = 4$ animals over two independent experiments). (E and F) Numbers indicate percentage of cells within the indicated gate.

Mafb-driven lineage tracing distinguishes monocytes and macrophages from other hematopoietic lineages

In the spleen of lineage-tracing mice, *Mafb*-mCherry was expressed abundantly in F4/80$^+$ macrophages, and expression of the lineage-tracing marker YFP was found in nearly all F4/80$^+$ macrophages but at background frequency among the classical DC subsets (Fig. 2 A and Fig. S1 A). In the brain, *Mafb*-mCherry was detectable in microglia, and YFP expression was found in nearly all such cells (Fig. 2 B and Fig. S1 B). In the blood, *Mafb*-mCherry expression was detectable only faintly (not depicted); however, YFP expression was observed in ∼10% of Ly-6C^{hi} monocytes and ∼40% of Ly-6C^{lo} monocytes (Fig. 2 C and Fig. S1 C). In contrast, we observed expression of the lineage-tracing marker YFP at a background frequency ranging from ∼1% to ∼6% in CD45$^-$ cells, B cells, and neutrophils (Fig. 2 C and Fig. S1 C), which may reflect some quantity of *Mafb* expression in the hematopoietic stem cell compartment (Sarrazin et al., 2009).

We detected no interpretable differences in gene expression between YFP$^+$ and YFP$^-$ Ly-6C^{lo} monocytes by microarray analysis (Fig. 2 D), suggesting that together they represent a single incompletely lineage-traced subset. We surmise that the short half-life (∼20 h at steady state) of Ly-6C^{hi} monocytes (Ginhoux and Jung, 2014) accounts for the lack of extensive lineage-tracing activity. Although gene expression microarray data show some up-regulation of the *Mafb* transcript at the Ly-6C^{hi} monocyte stage (Gautier et al., 2012), the lineage-tracing marker YFP would be detectable at the same stage only if transcription and translation of Cre, Cre-mediated recombination, and transcription, translation, and maturation of YFP

occur significantly within a day's span. By comparison, *Ccr2*-Cre^{ERT2}–based lineage tracing marks nearly all Ly-6C^{hi} monocytes, but *Ccr2* expression is up-regulated before commitment to the monocyte–macrophage lineage at the macrophage–DC progenitor stage, and lineage tracing is detectable in the common DC progenitor and its progeny (Croxford et al., 2015).

In the blood, Ly-6C^{lo} YFP^{+} monocytes showed greater intensities of YFP expression than did developing Ly-6C^{int} YFP^{+} monocytes; however, the perceived effect was subtle because the latter population was few in number (Fig. 2 E). In the gut lamina propria, Ly-6C^{hi} monocytes differentiate into CD64^{hi} Ly-6C^{lo} MHC-II^{+} macrophages through intermediary stages in a monocyte waterfall (Tamoutounour et al., 2012; Bain et al., 2014). We found that those intermediary stages also showed an intermediate frequency and intermediate intensities of YFP expression (Fig. 2 F and Fig. S1 D). Because YFP expression is under the control of a constitutive and ubiquitous promoter, these data suggest that cells adopting macrophage identity accumulated increasing concentrations of YFP until a steady-state concentration was reached late during differentiation.

Spleen and small intestinal macrophages express *Mafb* mRNA more abundantly than do macrophages in nearly any other organ (Gautier et al., 2012). To broaden our analysis, we used surface markers to identify BM and alveolar macrophages, which express little or no *Mafb* mRNA (Gautier et al., 2012). In some tissues, however, characteristic macrophage surface markers such as F4/80 cannot unambiguously distinguish those cells from other populations (Randolph and Merad, 2013). In the BM, we found that cells with the highest abundance of F4/80 showed substantial lineage tracing (Fig. 3 A and Fig. S1 E). In the lung, F4/80^{+} cells varied in Ly-6C expression; alveolar macrophages identified within the Ly-6C^{lo} fraction showed no detectable *Mafb*-mCherry expression but substantial lineage tracing, whereas a population of cells within the Ly-6C^{int} fraction expressing similar surface markers showed no detectable *Mafb*-mCherry expression and no lineage tracing (Fig. 3 B, Fig. S1 F, and not depicted). Thus, MafB-mCherry-Cre–based lineage tracing can identify macrophages even where those cells express little or no *Mafb* mRNA. Furthermore, this system can help to distinguish such populations from other cells that are similar in expression of surface markers such as F4/80.

Small peritoneal macrophages (SPMs) have been found to exhibit some characteristics of DCs, including dendritic morphology and expression of markers such as CD209 (DC-SIGN; Cain et al., 2013; Cassado et al., 2015). Although SPMs and DCs have been distinguished on the basis of M-CSFR or CD11c expression (Gautier et al., 2012; Cain et al., 2013), both populations are marked in lineage-tracing systems based on *Cx3cr1*-Cre or LysM-Cre (Cain et al., 2013). Using MafB-mCherry-Cre–based lineage tracing in conjunction with the *Zbtb46*-GFP reporter allele, we found a population of M-CSFR^{+} classical DCs that lacked expression of YFP (Fig. 3 C and Fig. S1 G).

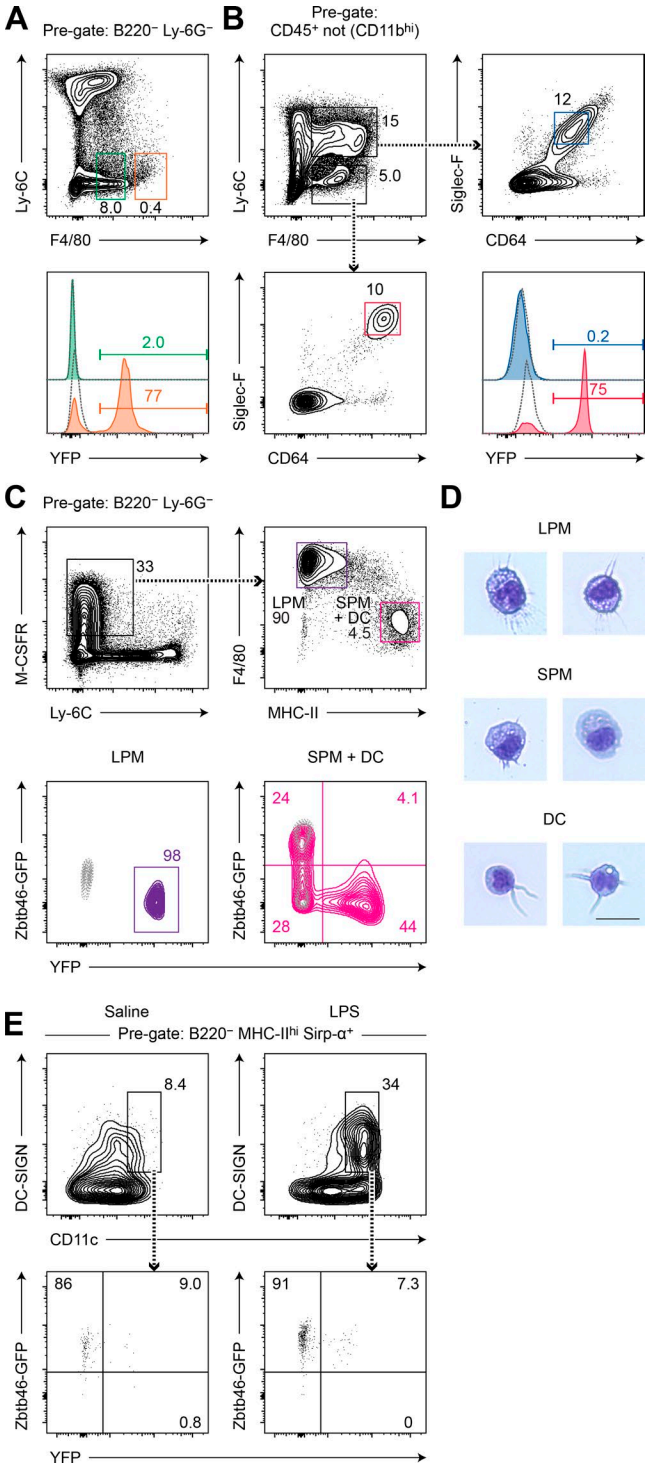

Figure 3. ***Mafb*–driven lineage tracing segregates macrophages from other populations.** (A) Macrophages in MafB-mCherry-Cre × R26-stop-YFP × *Zbtb46*-GFP mouse BM, identified by surface markers as indicated (orange) after pregating as in Fig. S1 E, are compared with F4/80^{+} cells of similar immunophenotype (green) for expression of lineage-tracing marker YFP. Shown is one representative sample ($n \geq 4$ animals over at least two independent experiments). (B) Alveolar macrophages in MafB-mCherry-Cre × R26-stop-YFP × *Zbtb46*-GFP mouse lung, identified by surface markers

After excluding those cells, large peritoneal macrophages (LPMs) and most SPMs expressed YFP (Fig. 3 C), and SPMs and DCs exhibited distinct morphologies (Fig. 3 D). In concordance with gene expression microarray data (Gautier et al., 2012), LPMs expressed greater quantities of *Mafb*-mCherry than did SPMs, and LPMs isolated from mice homozygous for the MafB-mCherry-Cre allele expressed *Mafb* mRNA as abundantly as did LPMs isolated from wild-type mice (not depicted).

In the skin-draining LN, cells that express DC-SIGN accumulate within the MHC-II^{hi} compartment after intravenous LPS injection (Cheong et al., 2010). Those cells express *Zbtb46*-GFP and fail to accumulate in Flt3L-deficient mice after treatment with LPS (Meredith et al., 2012; Satpathy et al., 2012a), which suggests that they are a population of classical DCs not derived from monocytes as was initially proposed. After LPS treatment of MafB-mCherry-Cre–based lineage–tracing mice carrying the *Zbtb46*-GFP allele, we confirmed that MHC-II^{hi} CD11c^{+} Sirp-α^{+} DC-SIGN^{+} cells in the inguinal LN were uniformly positive for expression of *Zbtb46*-GFP, but we did not observe expression of YFP in that population above a background frequency (Fig. 3 E and Fig. S1 H). These data suggest that such cells are not derived from a *Mafb*-expressing population.

LCs are *Zbtb46*-expressing cells marked by *Mafb*-driven lineage tracing

In the epidermis, expression of the surface marker epithelial cell adhesion molecule (EpCAM) is sufficient to distinguish LCs from classical DCs (Henri et al., 2010). However, in the skin-draining LN, radioresistant LCs are greatly outnumbered by donor-derived cells within the EpCAM^{+} compartment after reconstitution of irradiated mice using heterologous BM (Henri et al., 2010). Therefore, we assessed whether dual macrophage and DC characteristics observed in LCs could be explained by population heterogeneity at steady state.

Using MafB-mCherry-Cre–based lineage tracing, we first examined LCs in the inguinal LN. In that tissue, all EpCAM^{+} MHC-II^{+} cells were uniformly positive for expression of both *Zbtb46*-GFP and YFP, whereas EpCAM^{-} *Zbtb46*-GFP^{+} DC populations did not show YFP expression above background frequency (Fig. 4 A). Conversely, we found that almost all *Zbtb46*-GFP^{+} YFP^{+} cells were positive for expression of EpCAM and MHC-II, whereas cells that did not express both *Zbtb46*-GFP and YFP also did not express EpCAM (not depicted). These observations suggest that *Mafb*-expressing cells are the sole source of EpCAM^{+} cells in the skin-draining LN at steady state.

We next examined LCs in the epidermis (Fig. 4, B and C; Fig. S2, A and B). In that tissue, nearly all CD45^{+} MHC-II^{+} EpCAM^{+} CD24^{+} cells expressed abundant *Zbtb46*-GFP and YFP, although *Mafb*-mCherry expression did not reach the limit of detection (Fig. 4 B and not depicted). The presence of *Zbtb46*-GFP in skin LCs was unexpected because a previous study has found that the *Zbtb46* transcript is expressed at a similar abundance in skin LCs and splenic plasmacytoid DCs, much less than that in classical DCs (Miller et al., 2012; Satpathy et al., 2012b), and plasmacytoid DCs do not express detectable *Zbtb46*-GFP (Satpathy et al., 2012a). We also used anti-Zbtb46 antibody to compare protein expression in Zbtb46-sufficient (*Zbtb46*$^{+/+}$) and Zbtb46-deficient (*Zbtb46*$^{gfp/gfp}$) epidermal LCs (Fig. 4 C). Consistent with our earlier observation, we found that epidermal LCs expressed Zbtb46 protein. Thus, LCs are monocyte-derived cells that express Zbtb46 even at the tissue-resident stage.

Ly-6C^{+} monocyte-derived cells that infiltrate the lung are maturing macrophages

In the lung, administration of house dust mite (HDM) antigen induces an influx of cells that are distinguished from classical DCs by expression of CD64, Ly-6C, and MAR-1 (Plantinga et al., 2013). There has been disagreement as to whether these cells should be considered moDCs (Plantinga et al., 2013) or simply macrophages (Schlitzer et al., 2013). Thus, we used MafB-mCherry-Cre–based lineage tracing to study the infiltrating population after exposure to HDM antigen (Fig. 5 and Fig. S2 C). In the lung and mediastinal LN of HDM antigen–treated mice, we found that CD45^{+} MHC-II^{+} CD11c^{+} CD11b^{+} CD64^{+} cells did not express *Zbtb46*-GFP (Fig. 5, B, D, and E). Instead, we observed a continuum of Ly-6C expression within that population in the lung, with the Ly-6C^{hi} fraction expressing a lower abundance of YFP than did the Ly-6C^{lo} fraction (Fig. 5 B). Because YFP expression is controlled by a constitutive and ubiquitous promoter, these results favor the interpretation that infiltrating CD45^{+} MHC-II^{+} CD11c^{+} CD11b^{+} CD64^{+} cells are progressively adopting a macrophage identity.

as indicated (red) after pregating as in Fig. S1 F, are compared with F4/80^{+} Siglec-F^{+} CD64^{+} cells of similar immunophenotype (blue) for expression of YFP. Shown is one representative sample ($n \geq 4$ animals over at least two independent experiments). (C) MafB-mCherry-Cre × R26-stop-YFP × *Zbtb46*-GFP LPMs (purple) and SPMs (magenta), identified by surface markers as indicated after pregating as in Fig. S1 G, are compared for expression of *Zbtb46*-GFP and YFP in two-color histograms. Shown is one representative sample ($n \geq 3$ animals over at least two independent experiments). (A–C) Numbers indicate percentage of cells within the indicated gate, and dotted gray lines show fluorescent signal measured in non-mCherry and non-YFP control samples. (D) Macrophages (identified as *Zbtb46*-GFP^{-} Ly-6G^{-} CD11b^{+} *Mafb*-mCherry^{+} YFP^{+}, which were uniformly M-CSFR^{+}), distinguished as LPM (F4/80^{hi}) or SPM (F4/80^{lo}), and DCs (identified as *Zbtb46*-GFP^{+} CD11c^{+}) were sorted from the peritoneum of MafB-mCherry-Cre × R26-stop-YFP × *Zbtb46*-GFP mice and concentrated by Cytospin for morphological assessment by Wright–Giemsa staining. Shown are two representative cells for each population ($n = 3$ animals over two independent experiments). Bar, 20 µm. (E) DC-SIGN^{+} cells in the inguinal LNs of mice treated intravenously with vehicle (saline) or 10 µg LPS, identified by surface markers as indicated after pregating as in Fig. S1 H, are compared for expression of *Zbtb46*-GFP and YFP. Shown is one representative sample for each group ($n \geq 2$ animals per group over two independent experiments). Numbers indicate percentage of cells within the indicated gate.

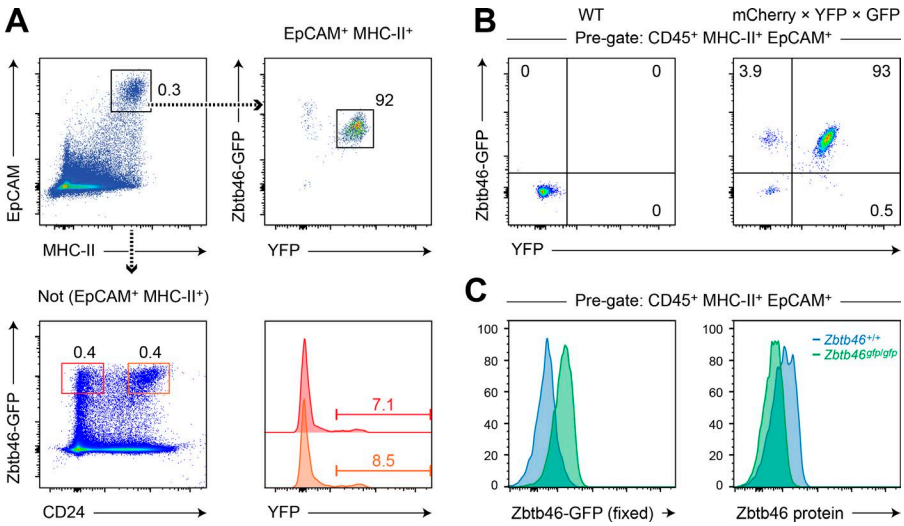

Figure 4. **LCs at steady state are marked by *Mafb*–driven lineage tracing but express *Zbtb46*.** (A) Migrated LCs in the inguinal LN of MafB-mCherry-Cre × R26-stop-YFP × *Zbtb46*-GFP mice are displayed for expression of *Zbtb46*-GFP and lineage-tracing marker YFP in a two-color histogram (top), and dermal DC populations in the same tissue identified by *Zbtb46*-GFP and CD24 are displayed for expression of YFP (bottom). Shown is one representative sample ($n \geq 4$ animals over at least two independent experiments). (B) LCs in the epidermis of wild-type or MafB-mCherry-Cre × R26-stop-YFP × *Zbtb46*-GFP (mCherry × YFP × GFP) mice, gated as in Fig. S2 A, are compared for expression of *Zbtb46*-GFP and YFP in two-color histograms. Shown is one representative sample per group ($n \geq 2$ animals per group over at least two independent experiments). (A and B) Numbers indicate percentage of cells within the indicated gate. (C) LCs in the epidermis of wild-type (*Zbtb46*$^{+/+}$) or Zbtb46-deficient (*Zbtb46*$^{gfp/gfp}$) mice, gated as in Fig. S2 B, are compared for expression of *Zbtb46*-GFP and Zbtb46 protein in one-color histograms. Shown is one representative sample per group ($n = 3$ animals per group over two independent experiments).

Collectively, our results demonstrate that the MafB-mCherry-Cre model is suitable for driving gene deletion specifically in macrophages, sparing deletion in DCs or neutrophils. MafB is also expressed outside the hematopoietic system, where our model may find additional applications. In the mouse endocrine pancreas, for example, MafB is expressed in mature α-cells but is also required for β-cell maturation (Artner et al., 2007). In the kidney, MafB is required for podocyte foot process formation (Moriguchi et al., 2006).

By using a lineage-tracing system based on MafB-mCherry-Cre, we found evidence that embryonic monocytes acquire Zbtb46 upon differentiation into LCs. In contrast, we found no evidence of similar cells in other organs at steady state (Fig. 6) or in the lung under inflammatory conditions. Instead, cells elicited by HDM antigen could be resolved into either *Zbtb46*-expressing DCs or CD64^{+} macrophages. Although we cannot exclude the possibility that *Mafb*-expressing lineages can give rise to *Zbtb46*-expressing progeny under conditions not examined here, it appears that LCs may be unique in acquiring these distinctive characteristics of macrophages and DCs.

MATERIALS AND METHODS

Mice

MafB-mCherry-Cre mice were maintained on the C57BL/6N background by interbreeding or by breeding to C57BL/6NJ mice (stock no. 005304; The Jackson Laboratory). To remove the neomycin resistance cassette, mice were bred to flippase (FLP) knock-in (B6N.129S4-*Gt(ROSA)26Sor*$^{tm1(FLP1)Dym}$/J) mice (stock no. 016226; The Jackson Laboratory) and then interbred to remove the FLP-expressing allele. The resulting strain is available at The Jackson Laboratory (stock no. 029664).

Zbtb46-GFP (B6.129S6(C)-*Zbtb46*$^{tm1.1Kmm}$) mice were generated by breeding 129S-*Zbtb46*^{tm1Kmm} mice (Satpathy et al., 2012a) to B6.C-Tg(CMV-cre)1Cgn/J mice (stock no. 006054; The Jackson Laboratory) to remove the neomycin resistance cassette. Offspring were bred to C57BL/6J mice for at least nine generations (removing the Cre-expressing transgene) and deposited at The Jackson Laboratory (stock no. 027618). R26-stop-YFP (B6.129X1-*Gt(ROSA)26Sor*$^{tm1(EYFP)Cos}$/J) mice were purchased from The Jackson Laboratory (stock no. 006148) and crossed to *Zbtb46*-GFP mice on the C57BL/6 background.

Experiments were performed using age-matched mice between 4 and 22 wk of age. Comparisons of treated mice with untreated mice used littermates for both groups; comparisons of fluorescent samples with nonfluorescent samples used, for the latter group, cells isolated from mice lacking the fluorescent markers of interest that were bred and maintained on the C57BL/6 background in the same facility. All mice were bred and maintained in a specific pathogen–free animal facility according to institutional guidelines and under protocols approved by the Animal Studies Committee of Washington University in St. Louis.

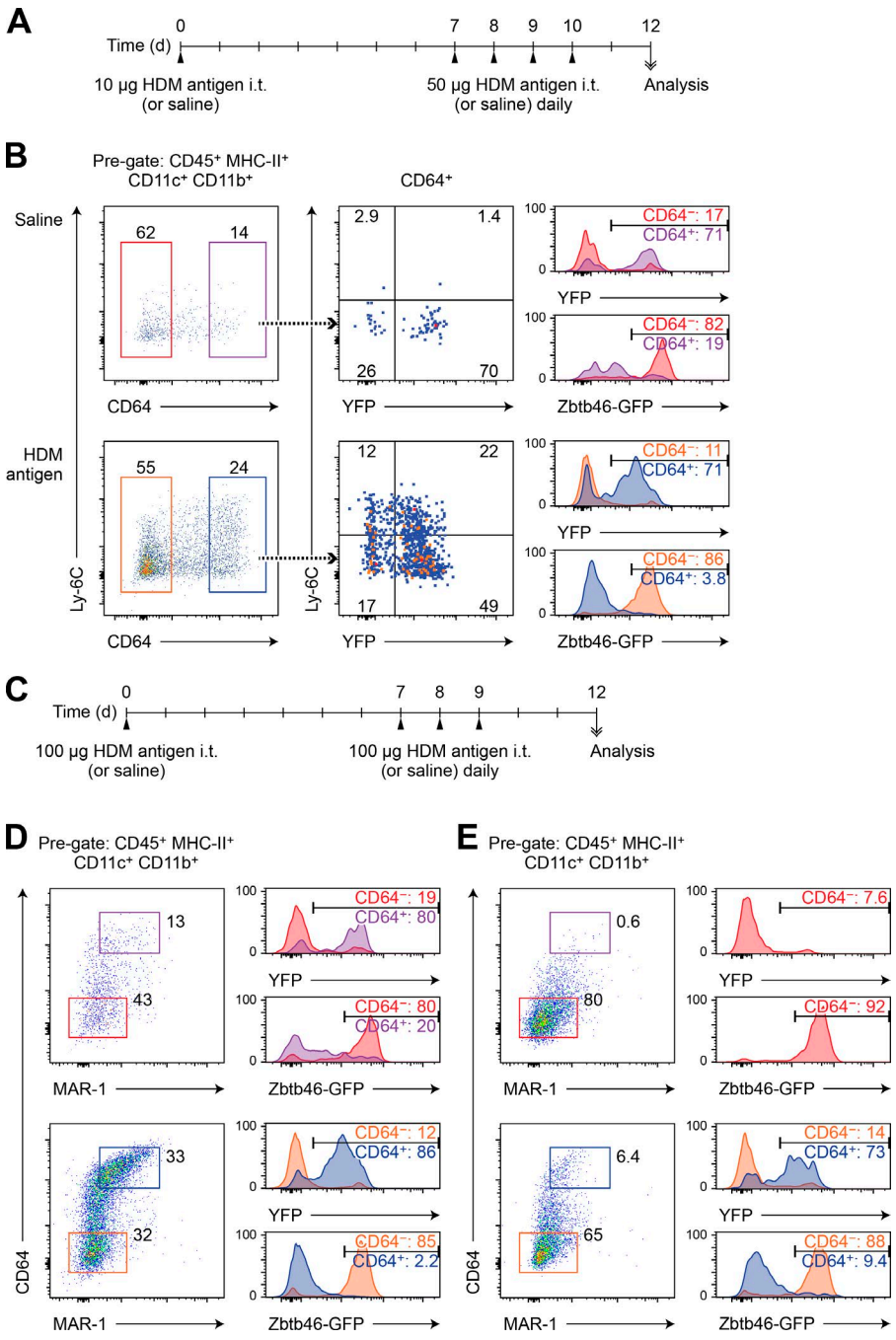

Figure 5. **Ly-6C+ monocyte-derived cells in the inflamed lung mature without expressing *Zbtb46*.** (A) Experimental outline for intratracheal (i.t.) sensitization and challenge of MafB-mCherry-Cre × R26-stop-YFP × *Zbtb46*-GFP mice using HDM antigen. (B) Classical DCs and monocyte-derived cells in the lung, identified by surface markers as indicated after pregating as in Fig. S2 C, are compared for expression of Ly-6C, lineage-tracing marker YFP, and *Zbtb46*-GFP after treatment with vehicle (saline) or HDM antigen following the schedule outlined in A. Shown is one representative sample ($n \geq 4$ HDM-treated animals over at least two independent experiments). Numbers indicate percentage of cells within the indicated gate. (C) Experimental outline for high-dose intratracheal sensitization and challenge of MafB-mCherry-Cre × R26-stop-YFP × *Zbtb46*-GFP mice using HDM antigen. (D and E) Classical DCs and monocyte-derived cells in the lung (D) or mediastinal LN (E), identified by surface markers as indicated, are compared for expression of YFP and *Zbtb46*-GFP after treatment with vehicle (saline) or HDM antigen following the schedule outlined in C. Shown is one representative sample (n = 2 HDM-treated animals over two independent experiments). Numbers indicate percentage of cells within the indicated gate.

Generation of the MafB-mCherry-Cre targeted mutation

P2A-FLAG-mCherry, T2A-Cre, and mouse MafB coding sequences were ligated serially into the pMSCV T2A-GFP retroviral overexpression vector, which was modified from the pMSCV IRES-GFP retroviral overexpression vector (Ranganath et al., 1998), to yield the pMSCV MafB-P2A-FLAG-mCherry-T2A-Cre retroviral overexpression vector. Primers used to amplify coding sequences by PCR are listed in Table S1.

The *Mafb* 3′–untranslated region (UTR) sequence was amplified from 129S6 genomic DNA using the following primers: 5′-ATTAGAATTCTTTCTGTGAGTCCTGGCGG-3′ and 5′-ATTAATCGATGGGGACTGCTTTTTTGTACAAACTTGTTGCCAGAGAATGTCCCAAAC-3′. Both the amplified 3′-UTR fragment and pMSCV MafB-P2A-FLAG-mCherry-T2A-Cre retroviral overexpression vector were digested using EcoRI and ClaI and then ligated together. A MafB-P2A-FLAG-mCherry-T2A-Cre-UTR fragment was

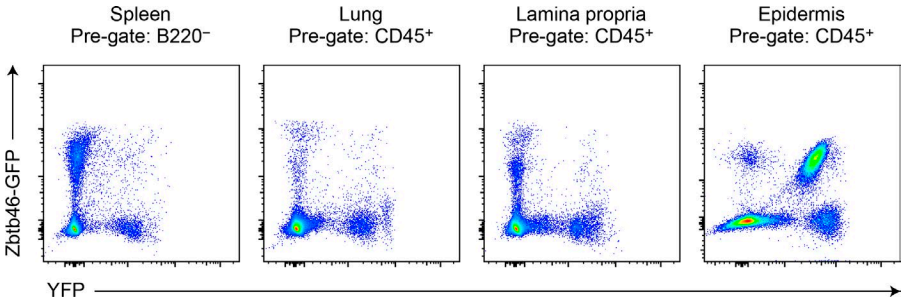

Figure 6. **A *Zbtb46*⁺ population marked by *Mafb*-driven lineage tracing is found in the skin but not in the spleen, lung, or small intestinal lamina propria at steady state.** B220⁻ cells from spleen samples in Fig. 2 A, CD45⁺ cells from lung samples in Fig. 3 B, CD45⁺ cells from small intestinal lamina propria samples in Fig. 2 F, and CD45⁺ cells from epidermis samples in Fig. 4 B are compared for expression of *Zbtb46*-GFP and lineage-tracing marker YFP in two-color histograms. Shown is one representative sample per tissue, each down-sampled to ∼5 × 10^4 cells.

released from the resulting vector by restriction digest using SacII, MluI, and Antarctic phosphatase (New England Biolabs, Inc.), and an ∼3-kb fragment containing *Mafb* 5′-UTR and upstream sequences was amplified from 129S6 genomic DNA and digested using MluI. The primers used to amplify the latter fragment were: 5′-ATTAAGATCTGGGGACAACTTTGT ATAGAAAAGTTGCGGAGTGTGGTGTTCTCTCT-3′ and 5′-CGTCTTCTCGTTCTCCAGGT-3′. The digested fragments were inserted into the pDONR (P4-P1R) plasmid (Invitrogen) by a modified BP recombination reaction in which incubation at room temperature was followed by addition of a supplemental buffer (10 mM $MgCl_2$ and 1 mM ATP) and T4 DNA ligase (New England Biolabs, Inc.) and incubation at 16°C for 5.5 h before addition of proteinase K solution to terminate the reaction. That reaction generated pENTR MafB-P2A-FLAG-mCherry-T2A-Cre-UTR.

A loxP-flanked fragment containing a neomycin resistance gene under the control of the *Pgk1* promoter (*Pgk1*-Neo^R) was released by restriction digest from the pLNTK-targeting vector (Gorman et al., 1996) and ligated into the pENTR lox-Puro vector (Iiizumi et al., 2006) to yield pENTR lox-rNeo, as previously described (Satpathy et al., 2012a). FLP recognition target (FRT) sites were introduced flanking the *Pgk1*-Neo^R cassette by site-directed mutagenesis using Pfu DNA polymerase (Agilent Technologies) to yield pENTR lox-FRT-rNeo. Flanking loxP sites were removed in a two-step process. First, the loxP/FRT-flanked *Pgk1*-Neo^R cassette was replaced with a synthetic DNA fragment purchased from Integrated DNA Technologies to yield an intermediate pENTR plasmid. Second, the intermediate pENTR plasmid was digested using MfeI-HF (New England Biolabs, Inc.) and BamHI, and then was ligated to a *Pgk1*-Neo^R fragment released from pENTR lox-FRT-rNeo using EcoRI and BamHI. Orientation of the synthetic fragment in the intermediate pENTR plasmid determined orientation of the *Pgk1*-Neo^R fragment in the final product, yielding either pENTR FRT-Neo or pENTR FRT-rNeo. The sequence of the synthetic fragment was: 5′-TACTACGCGGCCGCG AATTCGAAGTTCCTATTCCGAAGTTCCTATTCT CTAGAAAGTATAGGAACTTCATTAAGGGTTCCG GATCTATAGATCATGAGTGGGAGGAATGAGCTG GCCCTTAATTTGGTTTTGCTTGTTTAAATTATG ATATCCAACTATGAAACATTATCATAAAGCAAT AGTAAAGAGCCTTCAGTAAAGAGCAGGCATTTA TCTAATCCCACCCCACCCCCACCCCCGTAG CTCCAATCCTTCCATTCAAAATGTAGGTACTCT GTTCTCACCCTTCTTAACAAAGTATGACAGGAA AAACTTCCATTTTAGTGGACATCTTTATTGTTT AATAGATCATCAATTTCTGCAGACTTACAGCGG ATCCTTAATTCAATTGGAAGTTCCTATTCCGAA GTTCCTATTCTCTAGAAAGTATAGGAACTTCGA ATTCGAAGCGGCCGCCATCAT-3′.

Homology arms were amplified by PCR from C57BL/6 genomic DNA and the vector backbone was amplified from pDEST DTA-MLS (Iiizumi et al., 2006) using Q5 High-Fidelity DNA polymerase (New England Biolabs, Inc.) and primers listed in Table S2. A synthetic DNA fragment was purchased from Integrated DNA Technologies incorporating partial mCherry coding sequence, partial *Mafb* 3′-UTR sequence, and restriction sites for subsequent use. The sequence of the synthetic fragment was: 5′-GAGAGAGAC GCCTACAAGGTCAAGTGCGAGAAACTCGCCAAC TCCGGCTTCAGGGAGGCGGGCTCCACCAGCGAC AGCCCCTCCTCTCCTGAGTTCTTTCTGGTCGAG GGCAGCGGCGCCACGAACTTCAGCCTGCTGAAG CAAGCAGGAGATGTTGAAGAAAACCCCGGCCCT GATTACAAGGATGACGATGACAAGGTGAGCAAG GGCGAGGAGGATAACATGGCCATCATCAAGGAG TTCATGCGCTTCAAGGTGCACATGGAGGGCTCC GTGAACGGCCACGAGTTCGAGATCGAGGGCGAG GGCGAGGGCCGCCCCTACGAGGGCACCCAGACC GCCAAGCTGAAGGTGACCAAGGGTGGCCCCCTG CCCTTCGCCTGGGACATCCTGTCCCCTCAGTTC ATGTACGGCTCCAAGGCCTACGTGAAGCACCCC GCCGACATCCCCGACTACTTGAAGCTGTCCTTC CCCGAGGGATTTAAATGGGAGCGCGTGATGAAC TTCGAGGACGGCGGCGTGGTGACCGTGACCCAG GACTCCTCCCTGCAGGACGGCGAGTTCATCTAC AAGGTGAAGCTGCGCGGCACCAACTGATGTGGC TCTTCGCCCCCCTCGTCCTTCCCACTTCAGTTT

TAAGTTTTGTTGAGGGAAAGCGGCCGCTAAGGG AGAGACAGATGCCGAGATCCACATCGTGCAGGA GTGTGTCCTTTATTATTGTTGGGTCTTGGGGCC AAATTGACATACACACACCCACGACTGCTCCT-3′.

The amplified homology arm fragments, amplified vector backbone fragment, and synthetic fragment were assembled using Gibson Assembly Master Mix (New England Biolabs, Inc.) to yield the first intermediate targeting plasmid.

The first intermediate targeting plasmid was linearized using NotI and Antarctic phosphatase (New England Biolabs, Inc.) and then was used for ligation to an FRT-flanked *Pgk1*-Neo^R fragment released from pENTR FRT-Neo or pENTR FRT-rNeo using NotI and BsrGI (having ensured that the pENTR vector backbone would not interfere with ligation by digesting with NheI and AflII after digesting with NotI and BsrGI). The ligation yielded the second intermediate targeting plasmid.

An ∼1-kb fragment containing a portion of the 3′-UTR sequence was amplified from pENTR MafB-P2A-FLAG-mCherry-T2A-Cre-UTR using the following primers: 5′-GCTCGAGGATGGGGACTGAGAACTGTG AGTCCTGGCGGGT-3′ and 5′-CTGAAGTGGGAA GGACGAGG-3′. A fragment containing partial mCherry-T2A-Cre was released from pENTR MafB-P2A-FLAG-mCherry-T2A-Cre-UTR using SbfI-HF and EcoRI-HF (New England Biolabs, Inc.). The second intermediate targeting plasmid was linearized using CspCI and then was assembled with the amplified 3′-UTR fragment and the released mCherry-T2A-Cre fragment using Gibson Assembly Master Mix (New England Biolabs, Inc.) to yield the final targeting plasmid.

The linearized final targeting plasmid was electroporated into JM8.N4 mouse embryonic stem cells (C57BL/6N background; Knockout Mouse Project Repository). After selection with G418 (EMD Millipore), targeted clones were individually picked, expanded, and screened by Southern blot analysis. First, homologous recombination was identified using BamHI-digested genomic DNA and a digoxigenin-labeled 3′-probe amplified using the following primers: 5′-GGCACCAGGGGAATCTAGAA-3′ and 5′-ATGCTC CAAGACAACGATGC-3′. Next, homologous recombination was confirmed using SwaI-digested genomic DNA and a digoxigenin-labeled 5′-probe amplified using the following primers: 5′-CGCCTCCTATGTGCCATAAA-3′ and 5′-TTTCTCCAAAGCAAGCCCTG-3′.

Targeted clones were injected into blastocysts, and male chimeras were bred to female C57BL/6NJ mice (stock no. 000664; The Jackson Laboratory). Confirmation of germline transmission and determination of progeny genotype were performed by PCR using the following primers: 5′-CGAGAAGACGCAGCTCATTC-3′ (common forward), 5′-GAATAGGGAGTCTGGGCCAG-3′ (wild-type reverse), and 5′-CTTGGTCACCTTCAGCTTGG-3′ (mutant reverse). The expected sizes of amplicons were 424 bp (mutant) and 219 bp (wild type).

Cell preparation

Cheek pouch (submandibular) blood samples were collected using Microtainer tubes (BD) with EDTA after venipuncture using a 4-mm Golden Rod Animal lancet (MEDIpoint) per the manufacturer's instructions. Spleen samples were minced and digested in IMDM + 10% FCS (cIMDM) supplemented with 250 µg/ml collagenase B (Roche) and 30 U/ml DNase I (Sigma-Aldrich) for 30 min to 1 h at 37°C with stirring; LN samples were digested in the same manner without mincing. Microglia were isolated from brain by density gradient centrifugation using Percoll (P4937; Sigma-Aldrich), modifying a previously described method (Lee and Tansey, 2013) by substituting IMDM for DMEM/Nutrient Mixture F-12 (DMEM/F-12) and by additionally supplementing the dissociation medium with 1.7 mg/ml collagenase D (Roche), also omitting papain. In brief, brains were diced, dissociated in medium supplemented with Liberase TM (Roche), washed, filtered, and suspended in 37% Percoll. 70% Percoll was underlaid and 30% Percoll was overlaid. HBSS (Thermo Fisher Scientific) was overlaid, and samples were centrifuged before cells in the interface between 37% Percoll and 70% Percoll were recovered and washed. Peritoneum samples were harvested by injecting 10 ml PBS into the peritoneal cavity, agitating vigorously, and then collecting the injected fluid. BM samples were obtained by flushing the femur (or both the femur and the tibia) with magnetic-activated cell-sorting (MACS) buffer (PBS + 0.5% BSA + 2 mM EDTA). Epidermis samples were prepared by splitting ears into dorsal and ventral halves, incubating atop RPMI-1640 medium + 1.25 U/ml dispase (Roche) for 45 min to 1 h at 37°C, peeling and mincing epidermal sheets, and digesting in 0.05% trypsin-EDTA solution (Gibco) for 40 min at 37°C followed by repetitive pipetting. Lung samples were prepared after perfusion by injection of 5–10 ml PBS into the right ventricle; lung lobes were minced and digested in cIMDM supplemented with 2–4 mg/ml collagenase D and 30 U/ml DNase I for 1–2 h at 37°C with stirring. Small intestinal lamina propria samples were prepared as follows: after removal of Peyer's patches and fat, intestines were opened longitudinally, washed of fecal content, cut into pieces 1 cm in length, and incubated in HBSS + 15 mM Hepes + 5 mM EDTA at 37°C for 40 min with shaking at 250 rpm. Tissue suspensions were passed through a sieve, and the tissue pieces remaining were washed twice in PBS, minced, and incubated in cIMDM supplemented with collagenase B, collagenase D, and DNase I for 90 min at 37°C with stirring. Cell suspensions were pelleted, suspended in 40% Percoll, overlaid on 70% Percoll, and centrifuged for 20 min at 850 *g* before cells in the interface were recovered and washed in PBS.

To remove erythrocytes, samples were treated with ACK lysing buffer (0.15 M NH_4Cl + 10 mM $KHCO_3$ + 0.10 mM EDTA). Cells were filtered through 36-µm or 80-µm nylon mesh before resuspension in MACS buffer, and any cell counts were determined using a Vi-CELL analyzer (Beckman Coulter).

Antibodies and flow cytometry

Samples were stained in MACS buffer at 4°C in the presence of Fc Block (2.4G2; BD). The following antibodies purchased from BD, BioLegend, eBioscience, or Tonbo Biosciences were used to detect surface markers by flow cytometry: anti-CD3e (145-2C11) conjugated to biotin or FITC; anti-CD11b (M1/70) conjugated to eFluor 450, Pacific blue, FITC, PE, PE-Cy7, Alexa Fluor (AF) 700, or APC-Cy7; anti-CD11c (N418) conjugated to biotin, PerCP-Cy5.5, AF 647, or APC-Cy7; anti-CD11c (HL3) conjugated to Brilliant Violet 395; anti-CD19 (1D3) conjugated to biotin; anti-CD24 (M1/69) conjugated to PE, PE-Cy7, or AF 647; anti-CD43 (S7) conjugated to APC; anti-CD45 (30-F11) conjugated to eVolve 605; anti-CD45.2 (104) conjugated to Brilliant violet (BV) 605, PerCP-Cy5.5, APC, APC-Cy7, or APC–eFluor 780; anti-CD45R (B220; RA3-6B2) conjugated to eFluor 450, BV 510, PE-Cy7, AF 700, or APC-Cy7; anti-CD62L (MEL-14) conjugated to APC; anti-CD64 (X54-5/7.1) conjugated to AF 647 or APC; anti-CD102 (3C4 [MIC2/4]) conjugated to AF 647; anti-CD103 (M290) conjugated to BV 421; anti-CD115 (M-CSFR; AFS98) conjugated to BV 711, PerCP-eFluor 710, or PE; anti-CD117 (Kit; 2B8) conjugated to APC–eFluor 780; anti-CD135 (Flt3; A2F10) conjugated to APC; anti-CD170 (Siglec-F; E50-2440) conjugated to PE; anti-CD172a (Sirp-α; P84) conjugated to PerCP–eFluor 710, PE-Cy7, or APC; anti-CD207 (langerin; eBioL31) conjugated to biotin or PE; anti-CD226 (10E5) conjugated to PE; anti-CD326 (EpCAM; G8.8) conjugated to APC; anti-FcεRIα (MAR-1) conjugated to biotin; anti–Ly-6C (AL-21) conjugated to AF 700 or APC; anti–Ly-6C (HK1.4) conjugated to APC–eFluor 780; anti–Ly-6G (1A8) conjugated to biotin, BV 510, PerCP-Cy5.5, or PE; anti-NK1.1 (PK136) conjugated to eFluor 450; anti-F4/80 (BM8) conjugated to PE-Cy7 or APC–eFluor 780; anti–TER-119 conjugated to eFluor 450; and anti–MHC-II (I-A/I-E; M5/114.15.2) conjugated to BV 421, Pacific blue,V500, or BV 510. Streptavidin conjugated to eFluor 450 (eBioscience) or to BV 510 (BD) was also used for flow cytometry. To detect intracellular protein, samples were fixed, permeabilized, and washed using a Transcription Factor Buffer set (BD). The following antibody from BD was used after fixation and permeabilization: anti-Zbtb46 (U4-1374) conjugated to PE. Cells were analyzed using a FACSCanto II or FACSAria Fusion flow cytometer (BD), and data were analyzed using FlowJo software (Tree Star). All gating strategies incorporated size and doublet discrimination based on forward and side scatter parameters.

Gene expression microarray analysis

RNA was isolated from cells using an RNAqueous-Micro kit (Ambion), and target preparation was performed using the GeneChip WT Pico kit (Affymetrix) for hybridization to Mouse Gene 1.0 ST arrays (Affymetrix). Data were normalized, and expression values were modeled using ArrayStar 5 software (DNASTAR). Original microarray data have been deposited in Gene Expression Omnibus under accession no. GSE86596.

For principal component analysis, data were preprocessed using ArrayStar 5 software with robust multiarray average summarization and quantile normalization. Replicates were grouped by sample, and then, mean log-transformed expression values from each replicate group were exported in table format, imported into R software (R Foundation for Statistical Computing), mean-centered by gene, root-mean-square–scaled by sample, transposed, and subjected to principal component analysis computed by singular value decomposition without additional centering or scaling. Scores were plotted in R software.

Microscopy

Peritoneal macrophages and DCs were sorted using a FAC SAria Fusion flow cytometer (BD), concentrated by Cytospin, and stained with Wright–Giemsa stain using the Hema 3 system (Thermo Fisher Scientific). Bright-field images were captured at room temperature with a 40× objective lens using an EVOS FL Auto Imaging system (Invitrogen).

RT-PCR

For each biological replicate, peritoneum samples were isolated either from mice homozygous for the neomycin resistance cassette–deleted MafB-mCherry-Cre allele (*Mafb*$^{cre/cre}$) or from wild-type control mice. Between 1×10^5 and 2×10^5 LPMs were sorted from each sample using a FAC SAria Fusion flow cytometer (BD), RNA was isolated using an RNAqueous-Micro kit (Ambion) according to the manufacturer's instructions, first-strand cDNA was synthesized using qScript cDNA SuperMix (Quantabio), and quantitative analysis was performed using the LightCycler 480 system (Roche) with Luminaris Color HiGreen qPCR Master Mix (Thermo Fisher Scientific) and the following primer pairs: *Mafb* coding sequence (Sato-Nishiwaki et al., 2013), 5′-CGTCCAGCAGAAACATCACC-3′ and 5′-TCGCAC TTGACCTTGTAGGC-3′; and *Hprt1* (PrimerBank ID 7305155a1), 5′-TCAGTCAACGGGGGACATAAA-3′ and 5′-GGGGCTGTACTGCTTAACCAG-3′.

LPS

Mice were injected intravenously with 7.5 µg anti-CD209a (DC-SIGN; MMD3) antibody conjugated to eF660 (eBioscience) with or without 5 µg LPS (from *Escherichia coli* O55:B5; Sigma-Aldrich) diluted in 0.9% sodium chloride to a final volume of 200 µl, and then, inguinal LN samples were prepared 12 h after treatment.

HDM antigen

HDM antigen (*Dermatophagoides pteronyssinus* extracts; Greer Laboratories) was dissolved in PBS. Mice were sensitized and challenged intratracheally, as outlined in Fig. 5 (A or C), to induce allergic airway inflammation, and lung and mediastinal LN samples were prepared 2 or 3 d after final challenge.

Online supplemental material

Fig. S1 and S2 show flow cytometry gating strategies used to identify cell populations analyzed in this study. Tables S1 and

S2 detail primers used in the generation of the MafB-mCherry-Cre targeting plasmid.

ACKNOWLEDGMENTS

We thank Ansuman T. Satpathy for helpful discussions and critical reading, J. Michael White and the technical staff of the Transgenic Knockout Micro-Injection Core in the Department of Pathology and Immunology at Washington University School of Medicine for blastocyst injection, and the Genome Technology Access Center in the Department of Genetics at Washington University School of Medicine. The Genome Technology Access Center is partially supported by NCI Cancer Center Support grant no. P30 CA91842 to the Siteman Cancer Center and by the Institute of Clinical and Translational Sciences/Clinical and Translational Science Awards grant no. UL1 TR000448 from the National Center for Research Resources, a component of the U.S. National Institutes of Health (NIH) and NIH Roadmap for Medical Research.

This work was supported by the Howard Hughes Medical Institute (grant to K.M. Murphy), the NIH (grants nos. F30DK108498 to V. Durai, 1K08AI106953 to M. Haldar, and R01 AI049653 to G.J. Randolph), the Burroughs Wellcome Fund Career Award for Medical Scientists (to M. Haldar), and the National Science Foundation (grant no. DGE-1143954 to P. Bagadia).

The authors declare no competing financial interests.

Submitted: 27 April 2016

Accepted: 14 September 2016

REFERENCES

Abram, C.L., G.L. Roberge, Y. Hu, and C.A. Lowell. 2014. Comparative analysis of the efficiency and specificity of myeloid-Cre deleting strains using ROSA-EYFP reporter mice. *J. Immunol. Methods.* 408:89–100. http://dx.doi.org/10.1016/j.jim.2014.05.009

Anguille, S., E.L. Smits, E. Lion, V.F. van Tendeloo, and Z.N. Berneman. 2014. Clinical use of dendritic cells for cancer therapy. *Lancet Oncol.* 15:e257–e267. http://dx.doi.org/10.1016/S1470-2045(13)70585-0

Artner, I., B. Blanchi, J.C. Raum, M. Guo, T. Kaneko, S. Cordes, M. Sieweke, and R. Stein. 2007. MafB is required for islet β cell maturation. *Proc. Natl. Acad. Sci. USA.* 104:3853–3858. http://dx.doi.org/10.1073/pnas.0700013104

Artyomov, M.N., A. Munk, L. Gorvel, D. Korenfeld, M. Cella, T. Tung, and E. Klechevsky. 2015. Modular expression analysis reveals functional conservation between human Langerhans cells and mouse cross-priming dendritic cells. *J. Exp. Med.* 212:743–757. http://dx.doi.org/10.1084/jem.20131675

Bain, C.C., A. Bravo-Blas, C.L. Scott, E. Gomez Perdiguero, F. Geissmann, S. Henri, B. Malissen, L.C. Osborne, D. Artis, and A.McI. Mowat. 2014. Constant replenishment from circulating monocytes maintains the macrophage pool in the intestine of adult mice. *Nat. Immunol.* 15:929–937. http://dx.doi.org/10.1038/ni.2967

Bakri, Y., S. Sarrazin, U.P. Mayer, S. Tillmanns, C. Nerlov, A. Boned, and M.H. Sieweke. 2005. Balance of MafB and PU.1 specifies alternative macrophage or dendritic cell fate. *Blood.* 105:2707–2716. http://dx.doi.org/10.1182/blood-2004-04-1448

Bursch, L.S., L. Wang, B. Igyarto, A. Kissenpfennig, B. Malissen, D.H. Kaplan, and K.A. Hogquist. 2007. Identification of a novel population of Langerin$^+$ dendritic cells. *J. Exp. Med.* 204:3147–3156. http://dx.doi.org/10.1084/jem.20071966

Cain, D.W., E.G. O'Koren, M.J. Kan, M. Womble, G.D. Sempowski, K. Hopper, M.D. Gunn, and G. Kelsoe. 2013. Identification of a tissue-specific, C/EBPβ-dependent pathway of differentiation for murine peritoneal macrophages. *J. Immunol.* 191:4665–4675. http://dx.doi.org/10.4049/jimmunol.1300581

Cassado, A.A., M.R. D'Império Lima, and K.R. Bortoluci. 2015. Revisiting mouse peritoneal macrophages: heterogeneity, development, and function. *Front. Immunol.* 6:225. http://dx.doi.org/10.3389/fimmu.2015.00225

Caton, M.L., M.R. Smith-Raska, and B. Reizis. 2007. Notch–RBP-J signaling controls the homeostasis of CD8$^-$ dendritic cells in the spleen. *J. Exp. Med.* 204:1653–1664. http://dx.doi.org/10.1084/jem.20062648

Cheong, C., I. Matos, J.H. Choi, D.B. Dandamudi, E. Shrestha, M.P. Longhi, K.L. Jeffrey, R.M. Anthony, C. Kluger, G. Nchinda, et al. 2010. Microbial stimulation fully differentiates monocytes to DC-SIGN/CD209$^+$ dendritic cells for immune T cell areas. *Cell.* 143:416–429. http://dx.doi.org/10.1016/j.cell.2010.09.039

Chow, K.V., A.M. Lew, R.M. Sutherland, and Y. Zhan. 2016. Monocyte-derived dendritic cells promote Th polarization, whereas conventional dendritic cells promote Th proliferation. *J. Immunol.* 196:624–636. http://dx.doi.org/10.4049/jimmunol.1501202

Clausen, B.E., C. Burkhardt, W. Reith, R. Renkawitz, and I. Förster. 1999. Conditional gene targeting in macrophages and granulocytes using LysMcre mice. *Transgenic Res.* 8:265–277. http://dx.doi.org/10.1023/A:1008942828960

Cordes, S.P., and G.S. Barsh. 1994. The mouse segmentation gene *kr* encodes a novel basic domain-leucine zipper transcription factor. *Cell.* 79:1025–1034. http://dx.doi.org/10.1016/0092-8674(94)90033-7

Croxford, A.L., M. Lanzinger, F.J. Hartmann, B. Schreiner, F. Mair, P. Pelczar, B.E. Clausen, S. Jung, M. Greter, and B. Becher. 2015. The cytokine GM-CSF drives the inflammatory signature of CCR2$^+$ monocytes and licenses autoimmunity. *Immunity.* 43:502–514. http://dx.doi.org/10.1016/j.immuni.2015.08.010

Franklin, R.A., W. Liao, A. Sarkar, M.V. Kim, M.R. Bivona, K. Liu, E.G. Pamer, and M.O. Li. 2014. The cellular and molecular origin of tumor-associated macrophages. *Science.* 344:921–925. http://dx.doi.org/10.1126/science.1252510

Gautier, E.L., T. Shay, J. Miller, M. Greter, C. Jakubzick, S. Ivanov, J. Helft, A. Chow, K.G. Elpek, S. Gordonov, et al. Immunological Genome Consortium. 2012. Gene-expression profiles and transcriptional regulatory pathways that underlie the identity and diversity of mouse tissue macrophages. *Nat. Immunol.* 13:1118–1128. http://dx.doi.org/10.1038/ni.2419

Ginhoux, F., and S. Jung. 2014. Monocytes and macrophages: developmental pathways and tissue homeostasis. *Nat. Rev. Immunol.* 14:392–404. http://dx.doi.org/10.1038/nri3671

Ginhoux, F., F. Tacke, V. Angeli, M. Bogunovic, M. Loubeau, X.M. Dai, E.R. Stanley, G.J. Randolph, and M. Merad. 2006. Langerhans cells arise from monocytes in vivo. *Nat. Immunol.* 7:265–273. http://dx.doi.org/10.1038/ni1307

Ginhoux, F., M.P. Collin, M. Bogunovic, M. Abel, M. Leboeuf, J. Helft, J. Ochando, A. Kissenpfennig, B. Malissen, M. Grisotto, et al. 2007. Blood-derived dermal langerin$^+$ dendritic cells survey the skin in the steady state. *J. Exp. Med.* 204:3133–3146. http://dx.doi.org/10.1084/jem.20071733

Ginhoux, F., K. Liu, J. Helft, M. Bogunovic, M. Greter, D. Hashimoto, J. Price, N. Yin, J. Bromberg, S.A. Lira, et al. 2009. The origin and development of nonlymphoid tissue CD103$^+$ DCs. *J. Exp. Med.* 206:3115–3130. http://dx.doi.org/10.1084/jem.20091756

Gorman, J.R., N. van der Stoep, R. Monroe, M. Cogne, L. Davidson, and F.W. Alt. 1996. The Ig 3′ enhancer influences the ratio of Igκ versus Igλ B lymphocytes. *Immunity.* 5:241–252. http://dx.doi.org/10.1016/S1074-7613(00)80319-2

Greter, M., I. Lelios, P. Pelczar, G. Hoeffel, J. Price, M. Leboeuf, T.M. Kündig, K. Frei, F. Ginhoux, M. Merad, and B. Becher. 2012. Stroma-derived interleukin-34 controls the development and maintenance of langerhans cells and the maintenance of microglia. *Immunity.* 37:1050–1060. http://dx.doi.org/10.1016/j.immuni.2012.11.001

Guilliams, M., F. Ginhoux, C. Jakubzick, S.H. Naik, N. Onai, B.U. Schraml, E. Segura, R. Tussiwand, and S. Yona. 2014. Dendritic cells, monocytes and macrophages: a unified nomenclature based on ontogeny. *Nat. Rev. Immunol.* 14:571–578. http://dx.doi.org/10.1038/nri3712

Helft, J., J. Böttcher, P. Chakravarty, S. Zelenay, J. Huotari, B.U. Schraml, D. Goubau, and C. Reis e Sousa. 2015. GM-CSF mouse bone marrow cultures comprise a heterogeneous population of $CD11c^+MHCII^+$ macrophages and dendritic cells. *Immunity.* 42:1197–1211. http://dx.doi.org/10.1016/j.immuni.2015.05.018

Henri, S., L.F. Poulin, S. Tamoutounour, L. Ardouin, M. Guilliams, B. de Bovis, E. Devilard, C. Viret, H. Azukizawa, A. Kissenpfennig, and B. Malissen. 2010. $CD207^+$ $CD103^+$ dermal dendritic cells cross-present keratinocyte-derived antigens irrespective of the presence of Langerhans cells. *J. Exp. Med.* 207:189–206. http://dx.doi.org/10.1084/jem.20091964

Hertwig, P. 1942. Neue mutationen und koppelungsgruppen bei der Hausmaus. *Zeitschr. f. ind. Abst.- u. Vererbungslehre.* 80:220–246.

Hoeffel, G., Y. Wang, M. Greter, P. See, P. Teo, B. Malleret, M. Leboeuf, D. Low, G. Oller, F. Almeida, et al. 2012. Adult Langerhans cells derive predominantly from embryonic fetal liver monocytes with a minor contribution of yolk sac-derived macrophages. *J. Exp. Med.* 209:1167–1181. http://dx.doi.org/10.1084/jem.20120340

Hume, D.A., N. Mabbott, S. Raza, and T.C. Freeman. 2013. Can DCs be distinguished from macrophages by molecular signatures? *Nat. Immunol.* 14:187–189. http://dx.doi.org/10.1038/ni.2516

Iiizumi, S., Y. Nomura, S. So, K. Uegaki, K. Aoki, K. Shibahara, N. Adachi, and H. Koyama. 2006. Simple one-week method to construct gene-targeting vectors: application to production of human knockout cell lines. *Biotechniques.* 41:311–316. http://dx.doi.org/10.2144/000112233

Inaba, K., M. Inaba, N. Romani, H. Aya, M. Deguchi, S. Ikehara, S. Muramatsu, and R.M. Steinman. 1992. Generation of large numbers of dendritic cells from mouse bone marrow cultures supplemented with granulocyte/macrophage colony-stimulating factor. *J. Exp. Med.* 176:1693–1702. http://dx.doi.org/10.1084/jem.176.6.1693

Jakubzick, C., M. Bogunovic, A.J. Bonito, E.L. Kuan, M. Merad, and G.J. Randolph. 2008. Lymph-migrating, tissue-derived dendritic cells are minor constituents within steady-state lymph nodes. *J. Exp. Med.* 205:2839–2850. http://dx.doi.org/10.1084/jem.20081430

Jakubzick, C., E.L. Gautier, S.L. Gibbings, D.K. Sojka, A. Schlitzer, T.E. Johnson, S. Ivanov, Q. Duan, S. Bala, T. Condon, et al. 2013. Minimal differentiation of classical monocytes as they survey steady-state tissues and transport antigen to lymph nodes. *Immunity.* 39:599–610. http://dx.doi.org/10.1016/j.immuni.2013.08.007

Jovanovic, M., M.S. Rooney, P. Mertins, D. Przybylski, N. Chevrier, R. Satija, E.H. Rodriguez, A.P. Fields, S. Schwartz, R. Raychowdhury, et al. 2015. Dynamic profiling of the protein life cycle in response to pathogens. *Science.* 347:1259038. http://dx.doi.org/10.1126/science.1259038

Kaplan, D.H. 2010. In vivo function of Langerhans cells and dermal dendritic cells. *Trends Immunol.* 31:446–451. http://dx.doi.org/10.1016/j.it.2010.08.006

Kelly, L.M., U. Englmeier, I. Lafon, M.H. Sieweke, and T. Graf. 2000. MafB is an inducer of monocytic differentiation. *EMBO J.* 19:1987–1997. http://dx.doi.org/10.1093/emboj/19.9.1987

Kingston, D., M.A. Schmid, N. Onai, A. Obata-Onai, D. Baumjohann, and M.G. Manz. 2009. The concerted action of GM-CSF and Flt3-ligand on in vivo dendritic cell homeostasis. *Blood.* 114:835–843. http://dx.doi.org/10.1182/blood-2009-02-206318

Kissenpfennig, A., S. Henri, B. Dubois, C. Laplace-Builhé, P. Perrin, N. Romani, C.H. Tripp, P. Douillard, L. Leserman, D. Kaiserlian, et al. 2005. Dynamics and function of Langerhans cells in vivo: dermal dendritic cells colonize lymph node areas distinct from slower migrating Langerhans cells. *Immunity.* 22:643–654. http://dx.doi.org/10.1016/j.immuni.2005.04.004

Langlet, C., S. Tamoutounour, S. Henri, H. Luche, L. Ardouin, C. Grégoire, B. Malissen, and M. Guilliams. 2012. CD64 expression distinguishes monocyte-derived and conventional dendritic cells and reveals their distinct role during intramuscular immunization. *J. Immunol.* 188:1751–1760. http://dx.doi.org/10.4049/jimmunol.1102744

Lee, J.K., and M.G. Tansey. 2013. Microglia isolation from adult mouse brain. *Methods Mol. Biol.* 1041:17–23. http://dx.doi.org/10.1007/978-1-62703-520-0_3

Li, J.J., P.J. Bickel, and M.D. Biggin. 2014. System wide analyses have underestimated protein abundances and the importance of transcription in mammals. *PeerJ.* 2:e270. http://dx.doi.org/10.7717/peerj.270

Merad, M., M.G. Manz, H. Karsunky, A. Wagers, W. Peters, I. Charo, I.L. Weissman, J.G. Cyster, and E.G. Engleman. 2002. Langerhans cells renew in the skin throughout life under steady-state conditions. *Nat. Immunol.* 3:1135–1141. http://dx.doi.org/10.1038/ni852

Merad, M., P. Sathe, J. Helft, J. Miller, and A. Mortha. 2013. The dendritic cell lineage: ontogeny and function of dendritic cells and their subsets in the steady state and the inflamed setting. *Annu. Rev. Immunol.* 31:563–604. http://dx.doi.org/10.1146/annurev-immunol-020711-074950

Meredith, M.M., K. Liu, G. Darrasse-Jeze, A.O. Kamphorst, H.A. Schreiber, P. Guermonprez, J. Idoyaga, C. Cheong, K.H. Yao, R.E. Niec, and M.C. Nussenzweig. 2012. Expression of the zinc finger transcription factor zDC (Zbtb46, Btbd4) defines the classical dendritic cell lineage. *J. Exp. Med.* 209:1153–1165. http://dx.doi.org/10.1084/jem.20112675

Miller, J.C., B.D. Brown, T. Shay, E.L. Gautier, V. Jojic, A. Cohain, G. Pandey, M. Leboeuf, K.G. Elpek, J. Helft, et al. Immunological Genome Consortium. 2012. Deciphering the transcriptional network of the dendritic cell lineage. *Nat. Immunol.* 13:888–899. http://dx.doi.org/10.1038/ni.2370

Mollah, S.A., J.S. Dobrin, R.E. Feder, S.W. Tse, I.G. Matos, C. Cheong, R.M. Steinman, and N. Anandasabapathy. 2014. Flt3L dependence helps define an uncharacterized subset of murine cutaneous dendritic cells. *J. Invest. Dermatol.* 134:1265–1275. http://dx.doi.org/10.1038/jid.2013.515

Moriguchi, T., M. Hamada, N. Morito, T. Terunuma, K. Hasegawa, C. Zhang, T. Yokomizo, R. Esaki, E. Kuroda, K. Yoh, et al. 2006. MafB is essential for renal development and F4/80 expression in macrophages. *Mol. Cell. Biol.* 26:5715–5727. http://dx.doi.org/10.1128/MCB.00001-06

Plantinga, M., M. Guilliams, M. Vanheerswynghels, K. Deswarte, F. Branco-Madeira, W. Toussaint, L. Vanhoutte, K. Neyt, N. Killeen, B. Malissen, et al. 2013. Conventional and monocyte-derived $CD11b^+$ dendritic cells initiate and maintain T helper 2 cell-mediated immunity to house dust mite allergen. *Immunity.* 38:322–335. http://dx.doi.org/10.1016/j.immuni.2012.10.016

Poulin, L.F., S. Henri, B. de Bovis, E. Devilard, A. Kissenpfennig, and B. Malissen. 2007. The dermis contains $langerin^+$ dendritic cells that develop and function independently of epidermal Langerhans cells. *J. Exp. Med.* 204:3119–3131. http://dx.doi.org/10.1084/jem.20071724

Randolph, G., and M. Merad. 2013. Reply to: "Can DCs be distinguished from macrophages by molecular signatures?". *Nat. Immunol.* 14:189–190. http://dx.doi.org/10.1038/ni.2517

Ranganath, S., W. Ouyang, D. Bhattarcharya, W.C. Sha, A. Grupe, G. Peltz, and K.M. Murphy. 1998. GATA-3-dependent enhancer activity in IL-4 gene regulation. *J. Immunol.* 161:3822–3826.

Ryan, M.D., A.M. King, and G.P. Thomas. 1991. Cleavage of foot-and-mouth disease virus polyprotein is mediated by residues located within a 19 amino acid sequence. *J. Gen. Virol.* 72:2727–2732. http://dx.doi.org/10.1099/0022-1317-72-11-2727

Sallusto, F., and A. Lanzavecchia. 1994. Efficient presentation of soluble antigen by cultured human dendritic cells is maintained by granulocyte/macrophage colony-stimulating factor plus interleukin 4 and

downregulated by tumor necrosis factor α. *J. Exp. Med.* 179:1109–1118. http://dx.doi.org/10.1084/jem.179.4.1109

Sarrazin, S., N. Mossadegh-Keller, T. Fukao, A. Aziz, F. Mourcin, L. Vanhille, L. Kelly Modis, P. Kastner, S. Chan, E. Duprez, et al. 2009. MafB restricts M-CSF-dependent myeloid commitment divisions of hematopoietic stem cells. *Cell.* 138:300–313. http://dx.doi.org/10.1016/j.cell.2009.04.057

Sato-Nishiwaki, M., Y. Aida, S. Abe, Y. Shibata, T. Kimura, K. Yamauchi, H. Kishi, A. Igarashi, S. Inoue, M. Sato, et al. 2013. Reduced number and morphofunctional change of alveolar macrophages in MafB gene-targeted mice. *PLoS One.* 8:e73963. http://dx.doi.org/10.1371/journal.pone.0073963

Satpathy, A.T., W. Kc, J.C. Albring, B.T. Edelson, N.M. Kretzer, D. Bhattacharya, T.L. Murphy, and K.M. Murphy. 2012a. *Zbtb46* expression distinguishes classical dendritic cells and their committed progenitors from other immune lineages. *J. Exp. Med.* 209:1135–1152. http://dx.doi.org/10.1084/jem.20120030

Satpathy, A.T., X. Wu, J.C. Albring, and K.M. Murphy. 2012b. Re(de)fining the dendritic cell lineage. *Nat. Immunol.* 13:1145–1154. http://dx.doi.org/10.1038/ni.2467

Schaller, E., A.J. Macfarlane, R.A. Rupec, S. Gordon, A.J. McKnight, and K. Pfeffer. 2002. Inactivation of the F4/80 glycoprotein in the mouse germ line. *Mol. Cell. Biol.* 22:8035–8043. http://dx.doi.org/10.1128/MCB.22.22.8035-8043.2002

Schlitzer, A., N. McGovern, P. Teo, T. Zelante, K. Atarashi, D. Low, A.W. Ho, P. See, A. Shin, P.S. Wasan, et al. 2013. IRF4 transcription factor-dependent $CD11b^+$ dendritic cells in human and mouse control mucosal IL-17 cytokine responses. *Immunity.* 38:970–983. http://dx.doi.org/10.1016/j.immuni.2013.04.011

Schwanhäusser, B., D. Busse, N. Li, G. Dittmar, J. Schuchhardt, J. Wolf, W. Chen, and M. Selbach. 2011. Global quantification of mammalian gene expression control. *Nature.* 473:337–342. http://dx.doi.org/10.1038/nature10098

Seré, K., J.H. Baek, J. Ober-Blöbaum, G. Müller-Newen, F. Tacke, Y. Yokota, M. Zenke, and T. Hieronymus. 2012. Two distinct types of Langerhans cells populate the skin during steady state and inflammation. *Immunity.* 37:905–916. http://dx.doi.org/10.1016/j.immuni.2012.07.019

Silberberg-Sinakin, I., G.J. Thorbecke, R.L. Baer, S.A. Rosenthal, and V. Berezowsky. 1976. Antigen-bearing langerhans cells in skin, dermal lymphatics and in lymph nodes. *Cell. Immunol.* 25:137–151. http://dx.doi.org/10.1016/0008-8749(76)90105-2

Soucie, E.L., Z. Weng, L. Geirsdóttir, K. Molawi, J. Maurizio, R. Fenouil, N. Mossadegh-Keller, G. Gimenez, L. VanHille, M. Beniazza, et al. 2016. Lineage-specific enhancers activate self-renewal genes in macrophages and embryonic stem cells. *Science.* 351:aad5510. http://dx.doi.org/10.1126/science.aad5510

Srinivas, S., T. Watanabe, C.S. Lin, C.M. William, Y. Tanabe, T.M. Jessell, and F. Costantini. 2001. Cre reporter strains produced by targeted insertion of EYFP and ECFP into the ROSA26 locus. *BMC Dev. Biol.* 1:4. http://dx.doi.org/10.1186/1471-213X-1-4

Sultana, D.A., S. Tomita, M. Hamada, Y. Iwanaga, Y. Kitahama, N.V. Khang, S. Hirai, I. Ohigashi, S. Nitta, T. Amagai, et al. 2009. Gene expression profile of the third pharyngeal pouch reveals role of mesenchymal MafB in embryonic thymus development. *Blood.* 113:2976–2987. http://dx.doi.org/10.1182/blood-2008-06-164921

Szymczak-Workman, A.L., K.M. Vignali, and D.A. Vignali. 2012. Design and construction of 2A peptide-linked multicistronic vectors. *Cold Spring Harb. Protoc.* 2012:199–204. http://dx.doi.org/10.1101/pdb.ip067876

Tamoutounour, S., S. Henri, H. Lelouard, B. de Bovis, C. de Haar, C.J. van der Woude, A.M. Woltman, Y. Reyal, D. Bonnet, D. Sichien, et al. 2012. CD64 distinguishes macrophages from dendritic cells in the gut and reveals the Th1-inducing role of mesenteric lymph node macrophages during colitis. *Eur. J. Immunol.* 42:3150–3166. http://dx.doi.org/10.1002/eji.201242847

Wang, Y., K.J. Szretter, W. Vermi, S. Gilfillan, C. Rossini, M. Cella, A.D. Barrow, M.S. Diamond, and M. Colonna. 2012. IL-34 is a tissue-restricted ligand of CSF1R required for the development of Langerhans cells and microglia. *Nat. Immunol.* 13:753–760. http://dx.doi.org/10.1038/ni.2360

Zigmond, E., C. Varol, J. Farache, E. Elmaliah, A.T. Satpathy, G. Friedlander, M. Mack, N. Shpigel, I.G. Boneca, K.M. Murphy, et al. 2012. $Ly6C^{hi}$ monocytes in the inflamed colon give rise to proinflammatory effector cells and migratory antigen-presenting cells. *Immunity.* 37:1076–1090. http://dx.doi.org/10.1016/j.immuni.2012.08.026